XLVI CILAMCE
VITÓRIA - ES - BRAZIL - 2025
XLVI IBERO-LATIN AMERICAN CONGRESS ON COMPUTATIONAL METHODS IN ENGENEERING

The Extended Lumped Damage Mechanics in the failure analysis of anisotropic materials

Daniel V. C. Teles[1], David L. N. F. Amorim[1,2,3], Edson D. Leonel[1]

[1]*Graduate Program of Civil Engineering, São Carlos School of Engineering, University of São Paulo*
Av. Trabalhador são-carlense 400, Pq. Arnold Schimidt, São Carlos, 13566-590, São Paulo, Brazil
danielvcteles@usp.br, davidnf@academico.ufs.br, edleonel@sc.usp.br
[2]*Disaster Research Institute, Federal University of Sergipe*
Av. Marcelo Deda Chagas s/n, Rosa Elze, São Cristóvão, 49107-230, Sergipe, Brazil
davidnf@academico.ufs.br
[3]*Graduate Program of Civil Engineering, Federal University of Alagoas*
Av. Lourival Melo Mota s/n, Tabuleiro do Martins, Maceió, 57072-970, Alagoas, Brazil
davidnf@academico.ufs.br

Abstract. Many engineering materials exhibit anisotropic mechanical behaviour. The use of advanced and engineered materials to replace conventional engineering materials has triggered the requirement of many complex anisotropic mechanical models. Despite the elastic response of structures composed of anisotropic materials be studied since the last century, its failure analysis remains a significant challenge. In this study, the Extended Lumped Damage Mechanics (XLDM) approach addresses the material nonlinear behaviour of anisotropic materials. The XLDM combines fundamental concepts of fracture and damage mechanics and has proven effective in analysing structural failures. Besides, it has been implemented within a position-based finite element framework, which enables the failure analysis accounting for geometric nonlinearities.

Keywords: anisotropic materials, nonlinear behaviour, damage mechanics, finite element analysis, geometric nonlinearity.

1 Introduction

In light of growing environmental concerns, the use of low-carbon materials—such as timber—has become increasingly relevant in structural applications. This trend has renewed interest in modelling failure in anisotropic materials, particularly under complex loading conditions. Classical theories underpinning failure modelling include plasticity, continuum damage mechanics (CDM), and fracture mechanics, each offering complementary perspectives for representing nonlinear material behaviour.

Plasticity theory describes irreversible deformations once a yield threshold is reached, with well-established formulations for computational modelling of inelastic behaviour [1, 2]. CDM introduces internal variables to capture progressive stiffness degradation resulting from microstructural deterioration and has been formalised within the framework of thermodynamically irreversible processes [3, 4]. Fracture mechanics explicitly represents crack formation and propagation, whether through linear elastic models, cohesive fracture models [5, 6], or more recent phase-field approaches that allow for diffused crack representation without the need for discrete tracking [7, 8]. Despite their success, CDM and phase-field models may suffer from mesh dependency [9, 10] or demand fine spatial discretisation [11] unless enhanced by non-local or gradient-based regularisations [12–15].

To address some of these limitations, Lumped Damage Mechanics (LDM) was proposed by Flórez-López [16] to simulate localised degradation at discrete regions in frame structures. Drawing from both CDM and fracture mechanics, LDM has been successfully applied to nonlinear failure analysis in various structural configurations [17–22]. Building on this idea, the eXtended Lumped Damage Mechanics (XLDM) framework has been developed to handle failure in two-dimensional continua by introducing numerical extensometers into a finite element context [23, 24]. This strategy has proven effective in modelling failure in quasi-brittle materials using exponential stress-based degradation laws [25], reinforced composite structures [26], and isogeometric boundary element formulations [27]. Comparative studies with cohesive fracture models have demonstrated XLDM's mesh-objective behaviour due to its intra-element failure mechanism [28].

Recently, Teles et al. [29] extended the XLDM formulation within a position-based finite element method (FEM) framework [30, 31], enabling geometrically exact analysis with intrinsic treatment of large displacements and rotations. That study also included compressive damage modelling and embedded reinforcement via an intuitive implementation. The position-based FEM has demonstrated robust accuracy across several nonlinear applications [32–34]. This numerical framework serves as the computational basis for the contributions proposed herein.

This study advances the XLDM methodology in two main frontlines. First, it proposes an extensometer-free formulation, which eliminates the need for computing extensometer elongations and associated trigonometric projections, thereby improving computational performance and implementation clarity. Second, the XLDM framework is generalised to support the failure modelling of anisotropic materials.

2 Extensometer-free anisotropic XLDM within Position-based FEM

This study builds upon previous developments in the XLDM framework formulated within a position-based FEM [29]. Further details regarding the original XLDM formulation can be found in that reference. The present section focuses on two specific contributions: the extension of the XLDM to anisotropic materials and the formulation simplification by eliminating the need for numerical extensometers.

In XLDM, all material degradation is concentrated along the sides of each finite element. For each side, a localisation band is defined with thickness perpendicular to the element edge, as illustrated in Figure 1(a). These bands are then converted into displacement increments using trigonometric projections, and subsequently summed with the initial damaged configuration to obtain the current damaged configuration. In the extensometer-free version proposed herein, the Green–Lagrange strain tensor is computed directly from the nodal initial and current damaged configuration, bypassing the need to compute extensometer elongations. These three steps are summarised in Eq. (1):

$$\vec{u^d} = \begin{Bmatrix} s_{ij}e_i^{ij} - s_{il}e_i^{il} \\ -c_{ij}e_i^{ij} + c_{il}e_i^{il} \\ s_{ij}e_j^{ij} + s_{jk}e_j^{jk} \\ -c_{ij}e_j^{ij} - c_{jk}e_j^{jk} \\ -s_{lk}e_k^{lk} + s_{jk}e_k^{jk} \\ c_{lk}e_k^{lk} - c_{jk}e_k^{jk} \\ -s_{il}e_l^{il} - s_{lk}^{y}e_l^{lk} \\ c_{il}e_l^{il} + c_{lk}e_l^{lk} \end{Bmatrix} \quad ; \quad \vec{Y^d} = \vec{X^d} + \vec{u^d} \quad ; \quad \mathbf{E^d} = \frac{1}{2}\left(\left(\mathbf{A^d}\right)^T \cdot \mathbf{A^d} - \mathbf{I}\right) \tag{1}$$

in which e_i^{ij} and e_j^{ij} are the localisation bands at nodes i and j, respectively, in the side ij, and so on for the element sides; $\vec{X}^d$ and $\vec{Y}^d$ denote the initial and current damaged nodal positions, respectively; $\mathbf{A^d}$ is the damaged deformation gradient tensor and $\mathbf{E^d}$ is the corresponding Green–Lagrange strain tensor.

The evolution of the localisation bands is governed by a damage criterion. In this study, a bilinear softening law is adopted, as illustrated in Figure 1(b) and defined in Eq. (2):

$$g(\sigma, e) = \sigma - h(e) \leq 0 \quad ; \quad h(e) = \begin{cases} \sigma_{cr} - \left(\dfrac{\sigma_{cr} - \sigma_s}{e_s}\right) e & \text{if } e < e_s \\ \left(\dfrac{e - e_u}{e_s - e_u}\right) \sigma_s & \text{if } e_s \leq e < e_u \end{cases} \tag{2}$$

In this formulation, the stress has been taken as the normal projection of the Cauchy stress vector in the perpendicular direction to the element side, as damage evolution occurs along this direction. The criterion is evaluated independently for each band at the nodal level as follows:

$$g_i^{ij}(\sigma_i^{ij}, e_i^{ij}) = \sigma_i^{ij} - h_i^{ij}(e_i^{ij}) \leq 0 \quad \text{and} \quad g_j^{ij}(\sigma_j^{ij}, e_j^{ij}) = \sigma_j^{ij} - h_j^{ij}(e_j^{ij}) \leq 0 \tag{3}$$

where g_i^{ij} and g_j^{ij} are the local damage criteria, and h_i^{ij} and h_j^{ij} are the corresponding softening functions for nodes i and j of the localisation band ij; σ_i^{ij} and σ_j^{ij} are the projected Cauchy stress tensors; and e_i^{ij} and e_j^{ij} are the respective localisation band values.

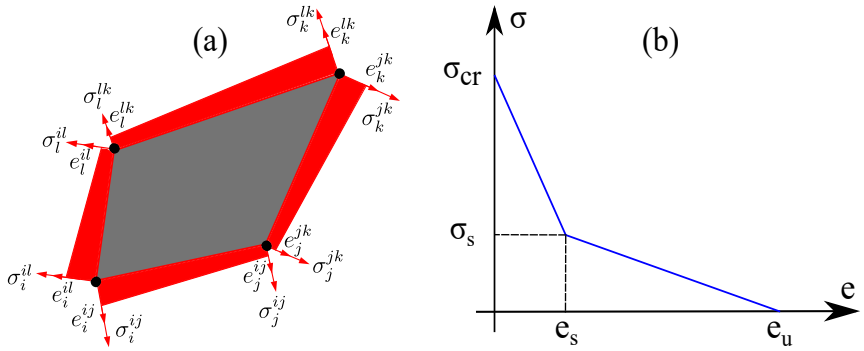


Figure 1. Localisation bands (a) and bilinear damage law (b).

A predictor–corrector scheme solves the damage evolution problem, as the band openings are not known a priori. Further details of the algorithmic implementation can be obtained in Teles et al. [29].

The Saint-Venant–Kirchhoff (SVK) constitutive model is adopted in this study, with the anisotropic stiffness tensor and its inverse, defined for a plane state, expressed respectively as:

$$\mathbb{C} = \begin{bmatrix} \mathbb{C}_{11} & \mathbb{C}_{12} & \mathbb{C}_{16} \\ \mathbb{C}_{12} & \mathbb{C}_{22} & \mathbb{C}_{26} \\ \mathbb{C}_{16} & \mathbb{C}_{26} & \mathbb{C}_{66} \end{bmatrix} \quad \text{and} \quad \mathbb{D} = \mathbb{C}^{-1} = \begin{bmatrix} \mathbb{D}_{11} & \mathbb{D}_{12} & \mathbb{D}_{16} \\ \mathbb{D}_{12} & \mathbb{D}_{22} & \mathbb{D}_{26} \\ \mathbb{D}_{16} & \mathbb{D}_{26} & \mathbb{D}_{66} \end{bmatrix} \tag{4}$$

where $\mathbb{C}_{ij}$ and $\mathbb{D}_{ij}$ represent the components of the stiffness and compliance tensors, respectively, with tensor symmetry already enforced. The components of the compliance tensor are given by:

$$\mathbb{D}_{11} = \frac{1}{E_1}, \quad \mathbb{D}_{12} = -\frac{\nu_{12}}{E_1}, \quad \mathbb{D}_{16} = \frac{\eta_{12,1}}{2E_1}, \quad \mathbb{D}_{22} = \frac{1}{E_2}, \quad \mathbb{D}_{26} = -\frac{\eta_{12,2}}{2E_2}, \quad \mathbb{D}_{66} = \frac{1}{2G_{12}} \tag{5}$$

in which E_1 and E_2 are the Young's moduli in the directions 1 and 2, respectively, ν_{12} is the Poisson's ratio, G_{12} is the shear modulus, $\eta_{12,1}$ and $\eta_{12,2}$ are the mutual influence coefficients in the directions 1 and 2, respectively. These last two coefficients are zero in isotropic and orthotropic materials. It is worth noting that the same parameters appear in the classical Hookean elasticity model.

In the present study, different parameter values are also assigned to the damage laws along each material direction to capture the anisotropic behaviour. This is consistent with the treatment of anisotropy in elasticity, where direction-dependent moduli are defined.

3 Applications

Two numerical applications are carried out to assess the performance of the XLDM formulation without the use of numerical extensometers in anisotropic problems. For all simulations, the convergence thresholds adopted for both the global equilibrium and local correction stages are set to 10^{-8}. Computations are performed on a personal computer with AMD Ryzen™ 9 7950X 16-Core @ 4.50 GHz processor and 64 GB of RAM.

3.1 Elastic anisotropy validation

The first application considers an anisotropic plate under uniform traction in plane stress condition, with geometry and boundary conditions shown in Figure 2. This case validates the proposed formulation in anisotropic elasticity, where strains are computed directly from nodal positions without extensometers. The analytical displacement field, according to Lekhnitskii et al. [35], is:

$$u_1 = \frac{1}{E_1} p x_1 + \frac{\eta_{12,1}}{E_1} p x_2 \qquad \text{and} \qquad u_2 = -\frac{\nu_{12}}{E_1} p x_2 \tag{6}$$

Material properties are: $E_1 = 124.04$ GPa, $E_2 = 10.09$ GPa, $\nu_{12} = 0.344$, $G_{12} = 6.03$ MPa, $\eta_{12,1} = 1.255$, and $\eta_{12,2} = -0.031$. A traction of 10 MPa has been applied within 100 steps to a mesh with 108 elements. Displacement results at the boundary coordinates (x_b) are shown in Figure 3, and the deformed shape in Figure 4 reflects the expected anisotropic response. The results exhibit excellent agreement with the analytical solution, confirming the correct implementation of anisotropic tensors in the XLDM framework.

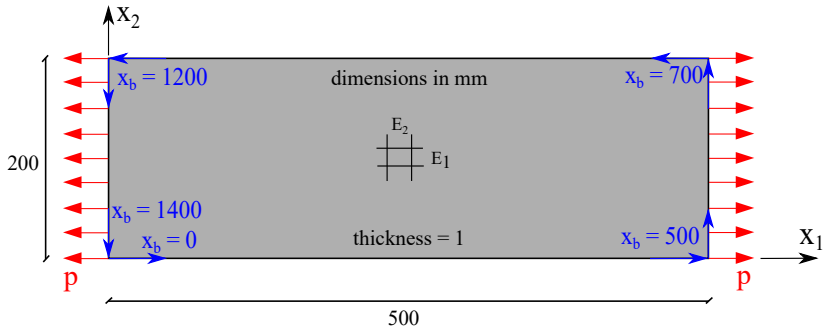


Figure 2. Geometry and boundary conditions.

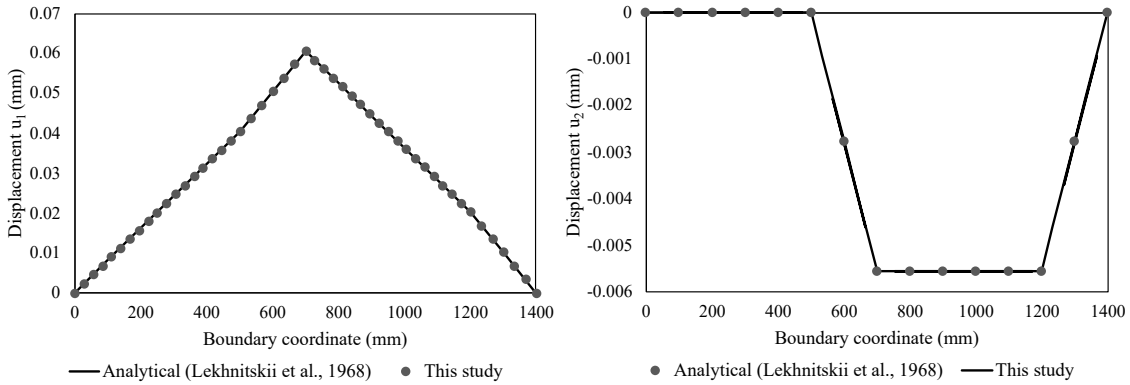


Figure 3. Displacement responses. Boundary coordinate starts at the lower left corner and runs in anticlockwise sense.

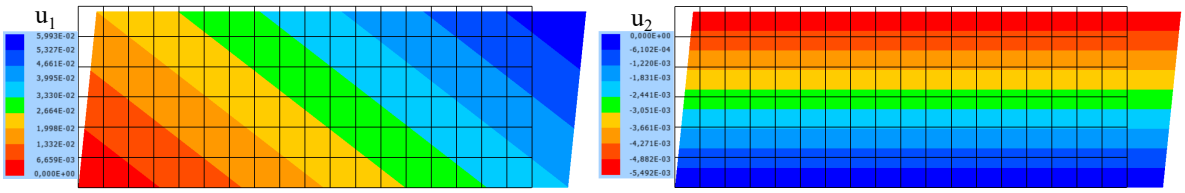


Figure 4. Final deformed shape

3.2 Three-point bending test

The second application examines the three-point bending behaviour of a Norway spruce (Picea abies) specimen. A pre-crack is introduced at the mid-span, and the specimen consists of three wooden sections: two outer parts bonded to a central portion with ARALDITE® AW106/953U epoxy resin, following the wood fibre orientation (Figure 5). This configuration ensures that principal stresses near the supports do not align with the longitudinal fibre direction, thus avoiding undesired crack propagation in those regions. The bonding interface is assumed to exhibit perfect adhesion. Details regarding the experimental setup can be found in Dourado et al. [36].

The material properties adopted are: $E_1 = 9900$ MPa, $E_2 = 334$ MPa, $\nu_{12} = 0.018$, $G_{12} = 610$ MPa, and fracture energy $G_f = 0.14481$ N/mm. Dourado et al. [36] recommend using an effective flexural modulus to account for shear deformation in larger specimens and based on the experimental compliance of 0.00465 mm/N and the specimen dimensions, an equivalent modulus $E_2 = 273.03$ MPa is obtained.

The problem is solved using a bilinear damage law, which yields more realistic behaviour for timber structures. The parameters used are: $\sigma_{cr} = 0.80$ MPa, $\sigma_s = 0.30$ MPa, $e_s = 0.13$ mm, and $e_u = 0.58$ mm.

Four meshes under plane stress condition discretise the domain. As shown in Figure 6(a), the central region is refined to better capture the damage localisation. The notch is represented by duplicating the central nodes along the notch depth. Numerical and experimental responses are shown in Figure 7(a), where the improved solution with mesh refinement is evident. In Figure 7(b), the two finest meshes yield nearly identical results, closely matching the experimental envelope. To highlight the localisation bands only central region are depicted in Figure 6(b), where consistent crack paths are observed in all meshes, demonstrating the robustness of the XLDM formulation.

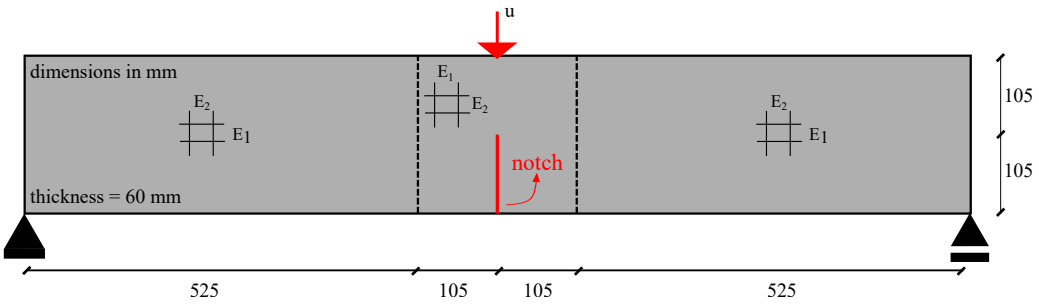


Figure 5. Geometry and boundary conditions of the three-point bending test.

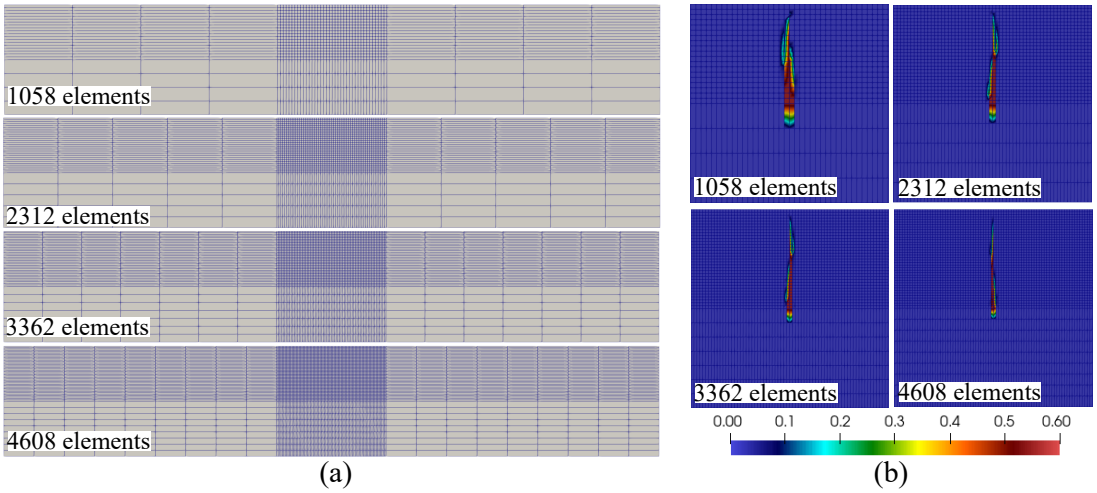


Figure 6. Meshes adopted in the three-point bending simulation.

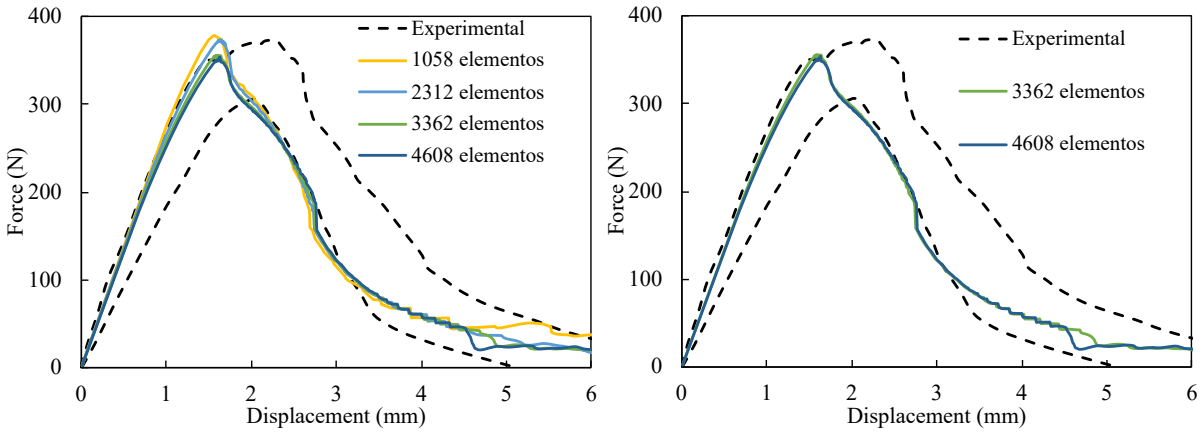


Figure 7. Numerical results: (a) all meshes; (b) comparison of the two finest meshes.

4 Conclusions

In the present study, the Extended Lumped Damage Mechanics (XLDM) approach is extended to account for anisotropic materials. The XLDM formulation is implemented within a position-based finite element framework, allowing for the analysis of structural failures while considering geometric nonlinearities. The accuracy of the proposed approach has been verified through two numerical applications: an elastic anisotropy validation and a three-point bending test on a Norway spruce specimen. The results demonstrate the effectiveness of the XLDM in capturing the nonlinear behaviour of anisotropic materials without relying on numerical extensometers, thus simplifying the computational process while maintaining accuracy.

Acknowledgements. The first author thanks the *Conselho Nacional de Desenvolvimento Científico e Tecnológico* (CNPq) for the financial support of his D.Sc. studies.

Authorship statement. The authors hereby confirm that they are the sole liable persons responsible for the authorship of this work, and that all material that has been herein included as part of the present paper is either the property (and authorship) of the authors, or has the permission of the owners to be included here.

References

[1] J. C. Simo and T. J. Hughes. *Computational inelasticity*. Springer Science & Business Media, 2006.
[2] E. A. Souza Neto, D. Peric, and D. R. J. Owen. *Computational methods for plasticity: theory and applications*. John Wiley & Sons, 2008.
[3] J. L. Chaboche. Continuous damage mechanics — a tool to describe phenomena before crack initiation. *Nucl. eng. des.*, vol. 64, pp. 233–247, 1981.
[4] B. Sun. A continuum model for damage evolution simulation of the high strength bridge wires due to corrosion fatigue. *J. Constr. steel res.*, vol. 146, pp. 76–83, 2018.
[5] A. Hillerborg, M. Modéer, and P.-E. Petersson. Analysis of crack formation and crack growth in concrete by means of fracture mechanics and finite elements. *Cem. concr. res.*, vol. 6, pp. 773–781, 1976.
[6] F. L. G. Santos and J. L. A. O. Sousa. A viscous-cohesive model for concrete fracture in quasi-static loading rate. *Eng. fract. mech.*, vol. 228, pp. 106893, 2020.
[7] P. Li, W. Li, B. Li, S. Yang, Y. Shen, Q. Wang, and K. Zhou. A review on phase field models for fracture and fatigue. *Eng. fract. mech.*, vol. 289, pp. 109419, 2023.
[8] R. de Borst and L. Chen. Phase-field modelling of cohesive interface failure. *Int. j. numer. methods eng.*, vol. 125, pp. 1–18, 2024.
[9] de R. Borst. Fracture in quasi-brittle materials: a review of continuum damage-based approaches. *Eng. fract. mech.*, vol. 69, pp. 95–112, 2002.
[10] R. H. J. Peerlings, de R. Borst, W. A. M. Brekelmans, and de J. H. P. Vree. Gradient enhanced damage for quasi-brittle materials. *Int. j. numer. methods eng.*, vol. 39, pp. 3391–3403, 1996.
[11] D. Proserpio, M. Ambati, L. D. Lorenzis, and J. Kiendl. A framework for efficient isogeometric computations of phase-field brittle fracture in multipatch shell structures. *Comput. methods appl. mech. eng.*, vol. 372, pp. 113363, 2020.
[12] B. Ahmed, G. Z. Voyiadjis, and T. Park. Local and non-local damage model with extended stress decomposition for concrete. *Int. j. damage mech.*, vol. 30, pp. 1149–1191, 2021.
[13] P. Lenz and R. Mahnken. Non-local integral-type damage combined to mean-field homogenization methods for composites and its parallel implementation. *Compos. struct.*, vol. 314, pp. 116911, 2023.
[14] J. Wang, L. H. Poh, and X. Guo. Localizing gradient damage model based on a decomposition of elastic strain energy density. *Eng. fract. mech.*, vol. 279, pp. 109032, 2023.
[15] L. Xue, X. Ren, and F. Freddi. Analytical solution of a gradient-enhanced damage model for quasi-brittle failure. *Appl. math. model.*, vol. 132, pp. 342–365, 2024.
[16] J. Flórez-López. Modelos de daño concentrados para la simulación numérica del colapso de pórticos planos. *Revista Internacional de Métodos Numéricos para Cálculo y Diseño en Ingeniería*, vol. 9, pp. 123–139, 1993.
[17] G. Kaewkulchai and E. B. Williamson. Beam element formulation and solution procedure for dynamic progressive collapse analysis. *Comput. struct.*, vol. 82, pp. 639–651, 2004.
[18] D. L. N. F. Amorim, S. P. B. Proença, and J. Flórez-López. Simplified modeling of cracking in concrete: Application in tunnel linings. *Eng. struct.*, vol. 70, pp. 23–35, 2014.
[19] J. A. V. Bazán, A. T. Beck, and J. Flórez-López. Random fatigue of plane frames via lumped damage mechanics. *Eng. struct.*, vol. 182, pp. 301–315, 2019.

[20] D. V. C. Teles, M. C. Oliveira, and D. L. N. F. Amorim. A simplified lumped damage model for reinforced concrete beams under impact loads. *Eng. struct.*, vol. 205, pp. 110070, 2020.
[21] K. O. Coelho, E. D. Leonel, and J. Flórez-López. A methodology to evaluate corroded RC structures using a probabilistic damage approach. *Comput. Concr. Int. J.*, vol. 29, pp. 1–14, 2022.
[22] J. M. J. Oliveira, C. S. Vieira, M. F. A. Silva, and D. L. N. F. Amorim. Fracture modelling of steel fibre reinforced concrete structures by the lumped damage mechanics: Application in precast tunnel segments. *Eng. struct.*, vol. 278, pp. 115487, 2023.
[23] D. L. N. F. Amorim, D. Piedade Neto, S. P. B. Proença, and J. Flórez-López. The extended lumped damage mechanics: A new formulation for the analysis of softening with fe size-independence. *Mech. res. commun.*, vol. 91, pp. 13–18, 2018.
[24] R. A. Picón, D. M. Santos, D. V. Teles, D. L. N. F. Amorim, X. Zhou, Y. Bai, S. P. B. Proença, and J. Flórez-López. Modeling of localization using nash variational formulations: The extended damage mechanics. *Eng. fract. mech.*, vol. 258, pp. 108083, 2021.
[25] D. V. C. Teles, R. N. Cunha, R. A. Picón, D. L. Amorim, Y. Bai, S. P. Proença, and J. Flórez-López. A new formulation of cracking in concrete structures based on lumped damage mechanics. *Struct. Eng. Mech.*, vol. 88, pp. 451–462, 2023.
[26] R. N. Cunha, D. L. N. F. Amorim, S. P. B. Proença, and J. Flórez-López. Modeling the initiation and propagation of complex networks of cracks in reinforced concrete plates. *Eng. struct.*, vol. 308, pp. 117993, 2024.
[27] D. C. Nardi and E. D. Leonel. An extended lumped damage mechanics igabem formulation for quasi-brittle material failure. *Eng. anal. bound. elem.*, vol. 169, pp. 105955, 2024.
[28] D. L. N. F. Amorim, R. Picón, C. S. Vieira, and J. Flórez-López. Intra-element versus inter-element crack propagation: the numerical extensometer approach. *J. Braz. Soc. Mech. Sci. Eng.*, vol. 46, pp. 360, 2024.
[29] D. V. C. Teles, D. L. N. F. Amorim, and E. D. Leonel. The failure prediction of reinforced composite quasi-brittle structures by an improved version of the extended lumped damage approach. *International Journal for Numerical Methods in Engineering*, vol. 126, n. 3, pp. e70006, 2025.
[30] J. Bonet, R. D. Wood, J. Mahaney, and P. Heywood. Finite element analysis of air supported membrane structures. *Comput. methods appl. mech. eng.*, vol. 190, pp. 579–595, 2000.
[31] H. B. Coda and M. Greco. A simple fem formulation for large deflection 2d frame analysis based on position description. *Comput. methods appl. mech. eng.*, vol. 193, pp. 3541–3557, 2004.
[32] H. B. Coda, C. C. L.-C. G. Bernardo, and R. R. Paccola. A fem formulation for the analysis of laminated and functionally graded hyperelastic beams with continuous transverse shear stresses. *Compos. struct.*, vol. 292, pp. 115606, 2022.
[33] P. R. P. Carvalho, H. B. Coda, and R. A. K. Sanches. A large strain thermodynamically-based viscoelastic–viscoplastic model with application to finite element analysis of polytetrafluoroethylene (ptfe). *Eur. j. mech. A solids*, vol. 97, pp. 104850, 2023.
[34] G. Avancini, A. Franci, S. Idelsohn, and R. A. K. Sanches. A particle-position-based finite element formulation for free-surface flows with topological changes. *Comput. methods appl. mech. eng.*, vol. 429, pp. 117118, 2024.
[35] S. G. Lekhnitskii, S. W. Tsai, and T. Cheront. *Anisotropic Plates*. Gordon and Breach Science Publishers, New York, 1968.
[36] N. Dourado, M. F. S. F. Moura, S. Morel, and J. Morais. Wood fracture characterization under mode i loading using the three-point-bending test. experimental investigation of picea abies l. *International Journal of Fracture*, vol. 194, pp. 1–9, 2015.